THE ASTROPHYSICAL JOURNAL, 551:565–575, 2001 April 10

A REDUCED MAGNETOHYDRODYNAMIC MODEL OF CORONAL HEATING IN OPEN MAGNETIC REGIONS DRIVEN BY REFLECTED LOW-FREQUENCY ALFVÉN WAVES

S. OUGHTON
Department of Mathematics, University College London, London WC1E 6BT, UK; sean@math.ucl.ac.uk

AND

W. H. MATTHAEUS, P. DMITRUK, L. J. MILANO, G. P. ZANK, AND D. J. MULLAN
Bartol Research Institute, University of Delaware, Newark, DE 19716; yswhm@bartol.udel.edu, pablo@bartol.udel.edu, zank@bartol.udel.edu, mullan@bartol.udel.edu
Received 2000 July 7; accepted 2000 November 9

ABSTRACT

A reduced magnetohydrodynamic (RMHD) description is employed to examine a suggestion made by W. H. Matthaeus and colleagues in 1999 that coronal heating might be sustained by a cascade of low-frequency MHD turbulence. Here RMHD simulations show that the low-frequency cascade to high transverse wavenumbers can be driven by an externally maintained flux of low-frequency propagating Alfvén waves, in combination with reflection caused by an inhomogeneous background medium. The simulations show that the suggestions made previously on the basis of a phenomenology are indeed realizable. In addition, the effect is seen to sensitively depend on the presence of reflection, as the background turbulence level needed to maintain the cascade can be sustained only when reflection is imposed. The steady level of turbulence is insensitive to the initial seed turbulence level (provided it is nonzero). Consequences of this model for realistic models of coronal heating in open field-line regions are discussed.

Subject headings: MHD — Sun: corona — Sun: magnetic fields — turbulence

1. INTRODUCTION

There are at present several theoretical models that employ transport and dissipation of magnetohydrodynamic (MHD) scale fluctuations to explain the heating of the open field-line corona. One class of models relies on high-frequency fluctuations (McKenzie, Banaszkiewicz, & Axford 1995; Axford & McKenzie 1997) that are easily transported through the lower corona and efficiently dissipated by cyclotron damping within 1–2 $R_\odot$. This mechanism requires generation of copious quantities of MHD waves at frequencies approaching the cyclotron frequency and is direct in the sense that the energy removed from the waves goes directly into heat. Another approach, known as "phase mixing" (Heyvaerts & Priest 1983), greatly amplifies dissipation of propagating waves through their interaction with a (quasi-static) sheared background medium. This essentially linear mechanism generates strong currents and enhanced heating in a wide variety of circumstances. Resonant absorption provides yet another way to heat coronal plasma using waves (Hollweg 1984; Davila 1987; Ofman, Davila, & Steinolfson 1994). A fourth approach, and the one we deal with in greater detail in this paper, involves driving of turbulence by reflection of low-frequency MHD waves. A distinguishing feature is that the wave energy is damped *indirectly* since it must pass through the turbulence to reach the dissipative scales. This model was presented recently in the context of a phenomenological description of both the turbulence and the wave reflection (Matthaeus et al. 1999; Oughton et al. 1999).

Coronal heating associated with nonlinear MHD effects, including cascade and reduced magnetohydrodynamic (RMHD) models, has been widely discussed in connection with closed field-line regions, especially loops (Gómez & Ferro-Fontán 1992; Heyvaerts & Priest 1992; Hendrix & van Hoven 1996; Einaudi et al. 1996; Dmitruk, Gómez, & DeLuca 1998). The critical difference in open-field regions is that the fluctuations can escape from the region in which heating is required through wave propagation. Since waves that are unidirectionally traveling exhibit no MHD nonlinear couplings in the incompressible limit (with uniform background fields), there is a possibility that energy escapes from the top rapidly enough that turbulence in the region of interest dies out in a finite time. This might occur because the couplings associated with the wave(s) that excite the turbulence are too weak to build up or replenish the turbulence before the wave energy transits the region of interest. This is essentially a key criticism of wave heating on open field lines as expressed, for example, by Parker (1991); however, Berger & Title (1996) later estimated that the wave flux from the photosphere was in fact adequate. In any case, the process of reflection provides a possible way out of this difficulty. If sufficient wave energy is reflected, the box will contain more equal amounts of counter-propagating fluctuations. These exhibit more robust nonlinear couplings than do waves propagating in one direction. Thus, reflection may cause a more rapid replenishment of the background turbulence.

In this paper, the nonlinear low-frequency cascade is represented by a driven, dissipative reduced MHD model at high Reynolds numbers. In contrast to our earlier treatment (Matthaeus et al. 1999), this permits a direct computation of the cascade, albeit in an idealized context, which supplants the earlier phenomenological formulation of turbulence heating rates. Since the latter presupposes a strong self-similar cascade, the present approach will permit a more sensitive evaluation of the competition between wave propagation and nonlinear effects. One of the central goals here is to investigate whether reflection can replenish requisite levels of turbulence needed to sustain significant rates of local heating. We will thus be able to corroborate our earlier conclusions concerning the dependence of steady heating rates on the strength of reflection. However, the

present model is still not a realistic model of the corona, as we are averaging effects such as reflection, transmission, and energy supply over the volume of our "box." This region is taken to be a representative sample of the corona, extending from above the transition region, perhaps from 1.05 to 2 $R_\odot$. The model is described in more detail below.

2. MODEL

The physical picture we consider has been described previously by Matthaeus et al. (1999) and is indicated in Figure 1. Alfvénic fluctuations, generated in the photosphere and/or chromosphere, are launched into an open field-line region of the corona. While propagating upward, they experience (non-WKB) reflections off the gradients in the background density and magnetic fields (Zhou & Matthaeus 1990b; Velli 1993). This yields a population of counter-propagating waves that couple nonlinearly with quasi–two-dimensional modes. The (driven) quasi–two-dimensional dynamics is such that energy cascades to small perpendicular length scales (relative to $\boldsymbol{B}_0$), where it is deposited as heat. The energy cascade is likely to involve the formation of current sheets and the (successive) reconnection of transverse magnetic islands (e.g., Hossain, Vahala, & Montgomery 1985; Matthaeus & Lamkin 1986). Allowance is also made for waves propagating out of the "top" of the heating region.

To fully investigate the feasibility of driving coronal heating in this way, the viability of a chain of events must be established, including (1) identification of an energy source, perhaps in the photospheric network, that can produce the requisite flux of low-frequency waves; (2) examination of the transport properties in the chromosphere and transition region to determine if a sufficient fraction of these waves can be transmitted to the corona; (3) determination that coronal turbulence and the nonlinear cascade can be sustained by driving with low-frequency waves from below; (4) that the level and type of reflections required for sustenance of turbulence is consistent with the large-scale structure of the corona; and (5) that appropriate kinetic processes in the coronal plasma are available to convert the MHD-scale turbulent energy into thermal degrees of freedom in such a way as to produce the observed features of coronal heating (see, e.g., Axford & McKenzie 1997; Leamon et al. 2000). Each aspect of this proposed process requires in-depth study. Here we concentrate on furthering our understanding of the third step in this process.

Specifically, we investigate some of the conditions for sustaining coronal heating using the low-frequency wave-driven quasi–two-dimensional turbulent cascade scenario outlined above. We find that reflection is essential if the system is to maintain a steady turbulent heating rate, as is a seed level of turbulence. However, as we will show, the time-asymptotic dissipation rate is quite insensitive to the initial turbulence level, as long as it is nonzero (as is likely to be the case above a turbulent photosphere). It is especially important that the model be able to replenish the zero-

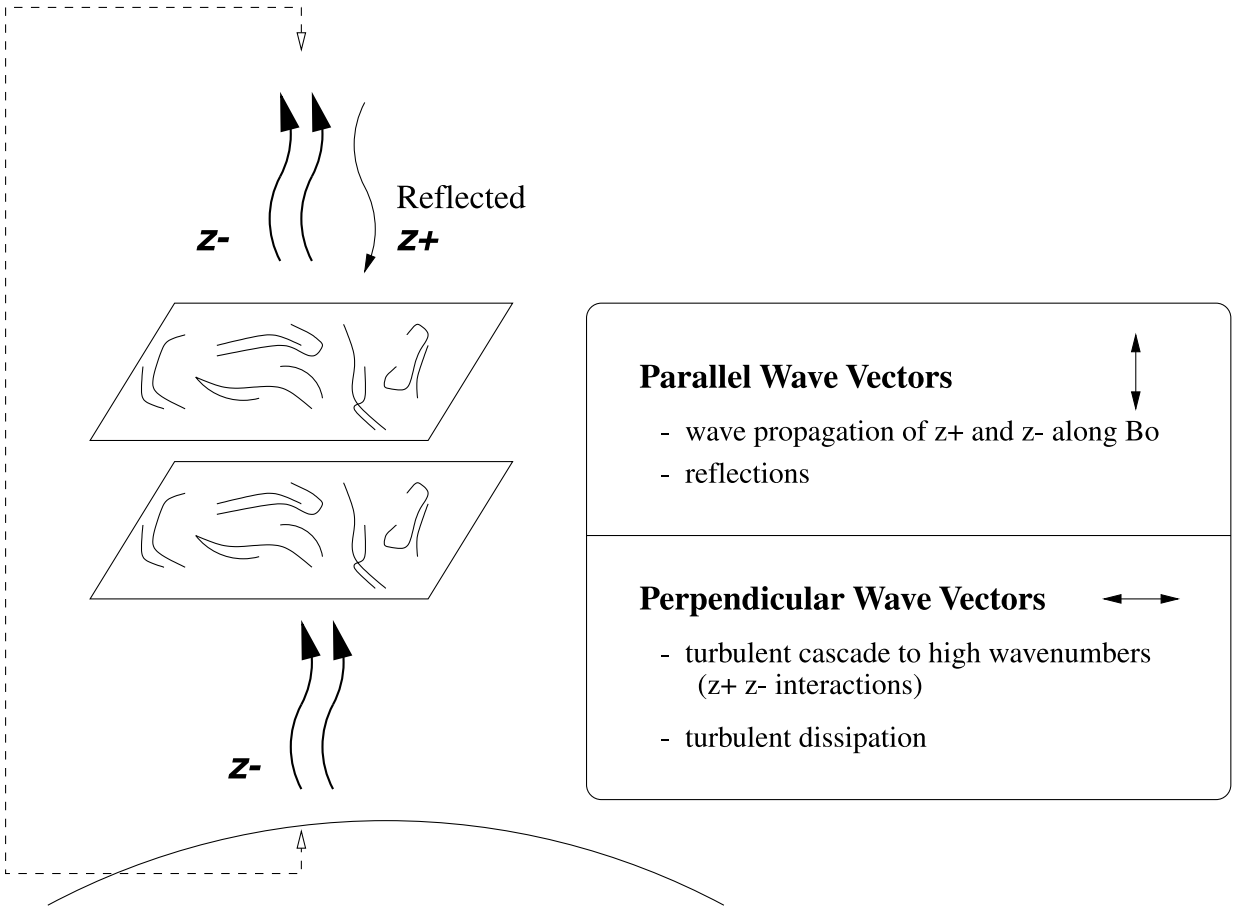

FIG. 1.—Sketch of the physics associated with the model for heating of coronal hole plasma. Dashed lines emphasize the periodic boundary conditions.

frequency portion of the fluctuations. Known as two-dimensional fluctuations, these excitations do not transport energy out of the box since they are nonpropagating (we are assuming that transport by the mean flow is negligible at these heights). Equally important is that two-dimensional fluctuations (in the incompressible limit) engage in a robust cascade process that is entirely insensitive to the strong vertical magnetic field. This corresponds to a large Alfvén speed that transports wave energy out of the box while also suppressing nonresonant nonlinear couplings. Two-dimensional fluctuations also act as catalysts for the resonant transfer of higher frequency fluctuations to small transverse scales (e.g., Shebalin, Matthaeus, & Montgomery 1983; Oughton, Priest, & Matthaeus 1994; Oughton, Ghosh, & Matthaeus 1998; Kinney & McWilliams 1998). All these effects are related to the nonpropagating character of the two-dimensional fluctuations, and, for these reasons, the very low parallel wavenumber (low-frequency) and zero-frequency parts of the local fluctuation spectrum may be expected to play a particularly important role in the type of heating model we discuss here. These are essentially the RMHD fluctuations.

We emphasize that our aim is to investigate one source of heating and not to rule out or deny the existence of other heating mechanisms. Indeed, we regard it as very likely that compressive wave activity is present and contributes to the heating at some level. Here, though, we assume that the perpendicular cascade produces the dominant form of dissipation, neglecting magnetoacoustic heating (including via shocks), parallel cyclotron damping, gravity waves, and other processes (e.g., Ofman & DeForest 2000; Ofman, Nakariakov, & Sehgal 2000; Ghosh et al. 1998a, 1998b; Gazol, Passot, & Sulem 1999; Khabibrakhmanov & Mullan 1994, 1997; Hollweg 1997).

3. REDUCED MAGNETOHYDRODYNAMIC FORMULATION

Reduced MHD, though not a replacement for a full MHD model, seems to be particularly appropriate in a low β_p corona having low fluctuation levels: $\delta B/B_0 \ll 1$, with β_p being the plasma beta factor (Mikić, Schnack, & Van Hoven 1989; Longcope & Sudan 1994; Einaudi et al. 1996; Hendrix & van Hoven 1996; Dmitruk & Gómez 1999). RMHD cascade (e.g., Montgomery 1982) is fueled by couplings that drive excitations principally to a high perpendicular wavenumber. That is, nonlinear RMHD spectral transfer produces structures having small spatial scale transverse to the mean (vertical) magnetic field $\boldsymbol{B}_0$. In a full (not reduced) MHD model, a strong perpendicular cascade of this type is expected when $\delta B/B_0$ is small. This has been shown in various simulation and analytical studies wherein the turbulence dynamically reorganizes to favor RMHD-type fluctuations (Montgomery & Turner 1981; Montgomery 1982; Shebalin et al. 1983; Carbone & Veltri 1990; Oughton et al. 1994, 1998; Matthaeus et al. 1996, 1998; Kinney & McWilliams 1998). It is also favored for low β_p in the nearly incompressible limit of fully compressible MHD (e.g., Zank & Matthaeus 1992; Bhattacharjee, Ng, & Spangler 1998). Thus, RMHD appears to capture the essential physics of the low-frequency waves and turbulence we wish to investigate. It also affords considerable advantages in numerical simplicity and efficiency.

The use of an RMHD description in models of the corona can be justified as follows. The RMHD formalism can be derived from compressible MHD under the assumptions of (1) low turbulent Mach number M_s, (2) low β_p, and (3) the restriction to low-frequency fluid-like behavior (Zank & Matthaeus 1992). Regarding (1) and (2), observational estimates in the lower corona (e.g., Hu, Esser, & Habbal 1997; Warren et al. 1997; Doyle et al. 1997) suggest that $u \approx 25$–35 km s^{-1}, $c_s \approx 115$ km s^{-1}, and $V_A \sim 1000$ km s^{-1} (or higher), yielding $M_s = u/c_s \approx 0.2$–0.3 and $\beta_p \propto c_s^2/V_A^2 \approx 0.01$. Thus, β_p is small and M_s small to moderate, so that our use of RMHD in the coronal context is consistent with the assumptions behind its derivation.

Note that this does *not* mean that acoustic activity cannot be present or is not important. It does imply that the RMHD limit should describe the leading-order nonlinearities, provided that all the activity is not acoustic to begin with. In keeping with many other coronal heating models (e.g., Axford & McKenzie 1997), we assume that the fluctuations launched from the network toward the corona are primarily Alfvénic in character (i.e., incompressive). Consequently, the fluctuations supplied to the coronal base are expected to have a significant incompressible component. Discussion regarding compressive effects can be found elsewhere (e.g., Ofman & DeForest 2000; Ofman et al. 2000).

To describe low-frequency RMHD couplings, it is useful to refer to a Fourier representation. A Fourier mode, e.g., a velocity field mode $\boldsymbol{v}(\boldsymbol{k})$, is said to be quasi–two-dimensional if both $\boldsymbol{k} \cdot \boldsymbol{B}_0 \approx 0$ and $\boldsymbol{v}(\boldsymbol{k}) \cdot \boldsymbol{B}_0 \approx 0$. While here we are interested in the nonlinear dynamics of such modes, it is worth emphasizing that even in the linear limit, incompressible quasi–two-dimensional modes are not, in general, waves in the usual sense. This is because fluctuations that are purely two-dimensional ($\boldsymbol{k} \cdot \boldsymbol{B}_0 = 0$) are strictly nonpropagating, having zero frequency (using the Alfvén wave dispersion relation). Fluctuations with nonzero but still very low frequency are significantly influenced by nonlinear couplings and are not expected to be accurately described as "waves."

The equations of RMHD are essentially those of incompressible two-dimensional MHD with allowance made for long-wavelength Alfvén wavelike couplings between the two-dimensional planes (Strauss 1976; Montgomery 1982; Zank & Matthaeus 1992). The retained dynamics satisfies $\tau_{nl} \lesssim \tau_A$, where $\tau_{nl} = 1/|k\boldsymbol{b}(\boldsymbol{k})|$ is the characteristic nonlinear timescale of a mode of wavenumber $k = |\boldsymbol{k}|$, and $\tau_A = 1/|\boldsymbol{k} \cdot \boldsymbol{B}_0|$ is its Alfvén period. In standard nondimensionalized units (with B_0 expressed in units of a characteristic Alfvén speed V_A), the RMHD equations for the evolution of the vorticity ω and the magnetic potential a are

$$\left(\frac{\partial}{\partial t} + \boldsymbol{v} \cdot \boldsymbol{\nabla}\right)\omega = \boldsymbol{b} \cdot \boldsymbol{\nabla} j + \nu \nabla_\perp^2 \omega + B_0 \frac{\partial j}{\partial z}, \tag{1}$$

$$\left(\frac{\partial}{\partial t} + \boldsymbol{v} \cdot \boldsymbol{\nabla}\right)a = \eta \nabla_\perp^2 a + B_0 \frac{\partial \psi}{\partial z}. \tag{2}$$

The equations are closed by noting that $\boldsymbol{\nabla} \cdot \boldsymbol{v} = 0$, $\omega = -\nabla_\perp^2 \psi$, and $\boldsymbol{v} = (\partial\psi/\partial y, -\partial\psi/\partial x, 0)$, with analogous expressions for the magnetic quantities, e.g., $j = -\nabla_\perp^2 a$. With the exception of the mean magnetic field, $\boldsymbol{B}_0 = B_0 \hat{\boldsymbol{z}}$, all quantities are functions of $\boldsymbol{r} = (x, y, z)$ and time, although the z dependence is "slow" (Montgomery 1982; Zank & Matthaeus 1992). The dissipation coefficients are equal to the inverse kinetic and magnetic Reynolds numbers: $\mathrm{Re} = 1/\nu$ and $R_m = 1/\eta$. Note that the final term in each equation

produces the long wavelength coupling of the two-dimensional planes.

The above standard RMHD equations require augmentation if they are to be applied within the context of the present model. We therefore introduce terms representing (in a volume-averaged sense) the forcing, reflection, and transmission of the waves that were included in our earlier phenomenological model (Matthaeus et al. 1999). Mean-square fluctuation amplitude is injected into a specified upward mode at rate F (corresponding to injection of kinetic plus magnetic energy at rate $F/4$). The outward propagating wave energy flux is reflected into inward propagating modes at rate R^-, with R^+ being the corresponding rate for reflection of inward waves into outward. All outward modes experience a reduction in their energy at the rate T, which simulates transmission of these waves out of the system. Denoting the energy (per unit mass) in outward waves by $E^- = \langle (\boldsymbol{v} - \boldsymbol{b})^2 \rangle$ and that in inward modes by $E^+ = \langle (\boldsymbol{v} + \boldsymbol{b})^2 \rangle$, we add additional terms to equations (1)–(2) so that the following energy equations are satisfied:

$$\frac{dE^-}{dt} = F - [R^- + T]E^- + R^+ E^+ , \tag{3}$$

$$\frac{dE^+}{dt} = R^- E^- - R^+ E^+ . \tag{4}$$

The total energy per unit mass is $E = (E^+ + E^-)/4$. The left-hand sides of these equations represent the dynamics embodied in equations (1)–(2). Note that the reflection and transmission terms in equations (3)–(4) correspond to additional reflection operators in equations (1)–(2).

It can be shown that the reflection rates $R^{\pm}$ are of order V_A/Δ, where Δ is a typical length scale for radial changes in the Alfvén velocity V_A (Hollweg 1981, 1996; Velli 1993; Zhou & Matthaeus 1990a), while the transmission rate is $T \sim V_A/L$, with L the box length in the parallel direction (Matthaeus et al. 1999). As noted above, RMHD dynamics requires $\tau_{nl} \lesssim \tau_A$ or, equivalently, $\sqrt{E}/\lambda_\perp \gtrsim V_A/L$, where $\lambda_\perp$ is a characteristic length scale for the quasi–two-dimensional component. Thus, for units where $\tau_{nl} = 1$, as is convenient in simulations and phenomenologies, one should require that $T \leq 1$. Strong reflection then corresponds to $R > 1$, with weak reflection occurring when $R < 1$.

4. RESULTS

The RMHD code can generate several types of runs of relevance to the physics of our proposed heating model. Some runs illustrate the basic properties of the code and are important for developing confidence in our approach.

The equations are solved using an (undealiased) pseudospectral code with second-order Runge-Kutta time stepping. Fourier expansions are used in all three directions with periodic boundary conditions applied. In the runs discussed herein, we always set $\nu = \eta$. With forcing, reflection, and dissipation "turned off," the code is initialized with broadband random velocity and magnetic fields characterized by power-law spectra. An undriven, ideal simulation of this type carried out for several tens of nonlinear times τ_{nl} indicates, as expected for a pseudospectral method, that the code accurately conserves both energy E and cross helicity $H_c = \langle \boldsymbol{v} \cdot \boldsymbol{b} \rangle$. Typically, conservation of E is accurate to better than one part in 10^4 for $t = 10\tau_{nl}$.

Another series of test runs includes no background turbulence. Instead, the code starts with an empty spectrum. Wave forcing is set to provide unit energy per unit time in a single upward-propagating mode, $\boldsymbol{k} = (1, 1, 1)$ in simulation units. With no dissipation and no reflection, the energy of the driven mode increases linearly in time. With transmission set to a fixed value T, but no reflection ($R = 0$), the driven mode saturates at the level $E_- = F/T$. In another test, the action of the numerical reflection algorithm is investigated by setting $R_+ = R_- = R$, $T = 0$, $F = 1$, and comparing the numerics with the analytic solution, which approaches equipartition. Finally, one can set nonzero values of F, R, and T and compare the numerical and analytic solutions.

The code agrees to near round-off levels with these test solutions. Notably, there is identically zero spectral transfer for all tests with zero background turbulence level. This is a consequence of two selection rules for generating turbulence: There are no nonlinear couplings (1) among unidirectionally propagating waves and/or (2) when the fluctuations reside at a single wavevector $\boldsymbol{k}$. These rules are one reason we have generally employed wave forcing, which is monochromatic and involves only upward-propagating modes, since one then has quantitative control over nonlinear couplings and the onset of spectral transfer. Note that we do not regard driving with a broadband upward flux as unrealistic. However, in that case, the driven waves would interact among themselves to drive turbulence. This would produce even stronger conclusions regarding the efficiency of the turbulent cascade. In employing monochromatic driving, we have adopted a more conservative approach and one that allows us to probe in greater detail the conditions for exciting and maintaining a strong nonlinear cascade and significant heating rates caused by turbulence.

4.1. *Steady Turbulence and Dissipation*

Our main results are for dissipative RMHD driven by a single monochromatic upward-propagating mode. Transmission and reflection are set to nonzero values. For the runs discussed in this subsection, the resolution is $256^2 \times 4$ with $\mathrm{Re} = R_m = 800$. The initial seed turbulence has unit energy and near-zero cross helicity, with a broadband spectrum where all k_z modes with $2 \leq k_\perp \leq 6$ are excited.

Using this approach, we performed two long simulations out to a final time of $t = 500$, where the unit of time is an Alfvén crossing time for the box. (Each of these runs required more than 35 days of CPU time on a 600 MHz Alpha processor.) Both runs were at $F = 1$, $T = 0.3$, but differed in the value of R used, either $\frac{1}{2}$ or 1. Initially, the driving pumps up the (1, 1, 1) mode as the background turbulence experiences a period of rapid initial decay and then a strong growth.

After $t \approx 20$, the system begins to approach a steady state, with the turbulent decay approximately balanced by new energy supplied by the driven wave and by its reflection, the downward propagating mode with the same $\boldsymbol{k}$. Figure 2 illustrates this scenario for the $R = \frac{1}{2}$ run. Shown are time histories of total energy E, the normalized cross helicity $\sigma_c = (E^+ - E^-)/(E^+ + E^-)$, and the mean-square current density $\langle j^2 \rangle$. The final panel of the figure compares the time-dependent turbulent dissipation rate (ϵ_{turb}) with the rate of energy loss caused by transmissions. It is evident that the latter two quantities sum on average to the supplied energy flux $F = 1$. However, at any particular time the

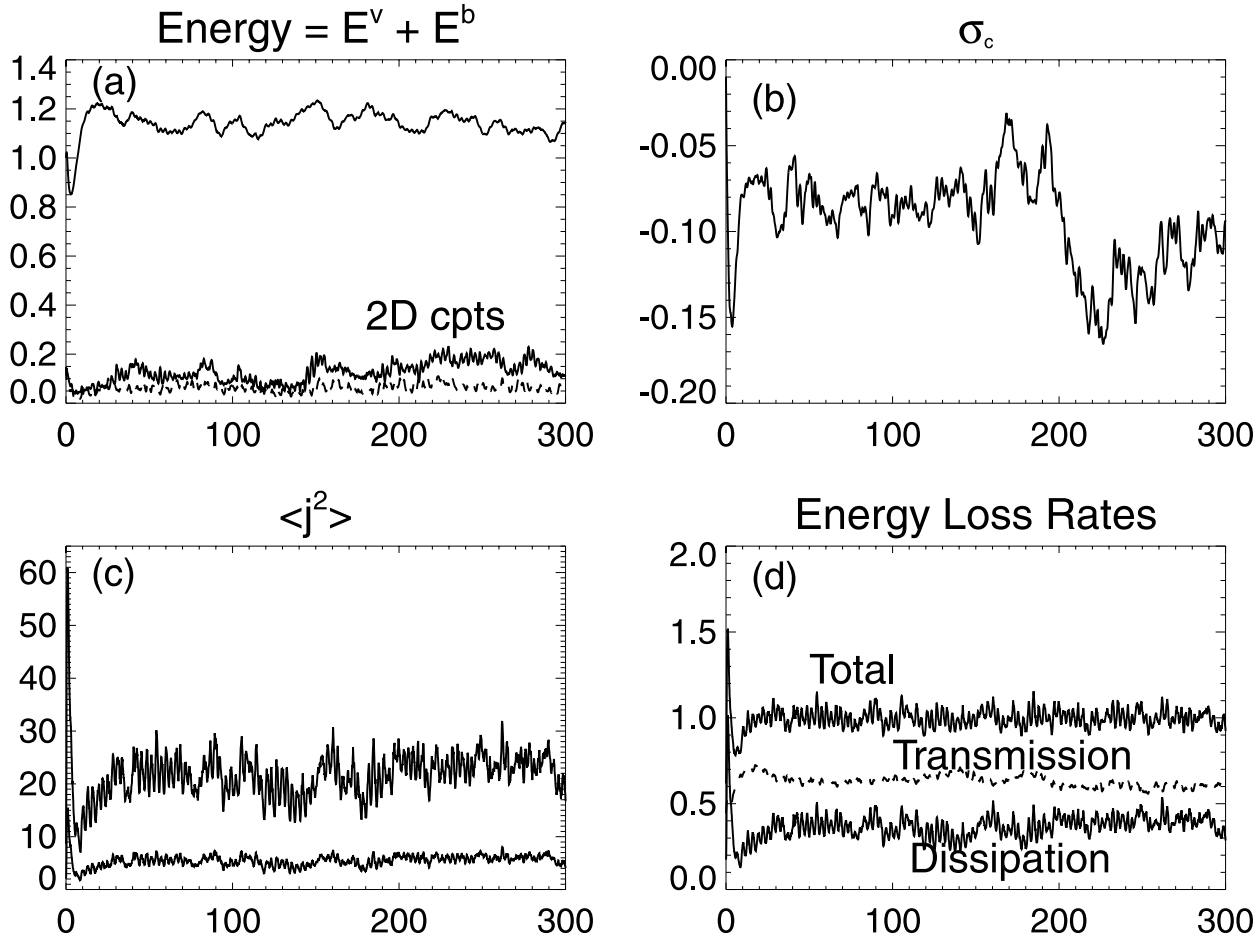

FIG. 2.—Time histories of (*a*) total turbulence energy and the two-dimensional contributions to turbulence energy (E^b = solid), (*b*) normalized cross helicity $\sigma_c = (E^+ - E^-)/(E^+ + E^-)$, (*c*) mean-square current density $\langle j^2 \rangle$, with its two-dimensional component shown as the lower trace, and (*d*) energy loss rates via dissipation, transmission (*dashed line*), and their sum. Results out to $t = 500$ look very similar to the steady phase shown here. N.B.: Figs. 2–6 all employ data from the "primary" $R = \frac{1}{2}$, $256^2 \times 4$ run.

turbulence energy may vary from its average and the rates of loss and supply are not expected to precisely balance. A notable and central feature of Figure 2 is that the dissipation rate caused by turbulence corresponds to a significant fraction of the energy supply rate. An estimate of the average efficiency of turbulent dissipation is given by $\langle \epsilon_{\rm turb} \rangle / F$, which is about 25% in this case. In a more realistic coronal model, this would signify that one-fourth of the input wave energy flux ends up heating the plasma lying within the simulation domain. Results from the companion high-resolution run (with $R = 1$), as well as various runs carried out at lower resolutions (usually $64^2 \times 4$), confirm this general behavior for a variety of parameters. We now turn to a more detailed look at the properties of the steady driven turbulence.

4.2. *Properties of the Turbulence*

Wavenumber spectra characterize the distribution of fluctuation energy over scale. Below, we consider the reduced and two-dimensional spectra at a particular time in the steady turbulence phase of the simulation. Spectra at other times during this phase are similar. (All diagnostics in this subsection employ data from the driven $R = \frac{1}{2}$ high-resolution run.)

Figure 3 shows two energy spectra of the kinetic and magnetic fluctuations at $t = 100$. The first of these is the reduced magnetic spectrum, $E^r(k_\perp) = \sum_{k_z} E(k_\perp, k_z)$, which is a function of a perpendicular wavenumber. For comparison, we also show the spectrum associated with the strictly two-dimensional fluctuations: $E^{2D}(k_\perp) = E(k_\perp, k_z = 0)$. Two features are evident. First, although the energy has been supplied at long wavelength ($k_\perp = \sqrt{2}$), the fluctuation spectrum is broadband and nearly monotonic decreasing. There is a suggestion of an inertial range of modest bandwidth since the slope passes through a region of approximately $k^{-5/3}$ behavior. Note that there is no strong spectral feature corresponding to the forcing wavenumber. This indicates that spectral transfer is efficiently coupling the input wavenumber to the full set of wavenumbers participating in the cascade. A second noteworthy feature is that the two-dimensional spectrum is maintained at a significant level. It includes no directly forced modes and is driven only indirectly through spectral transfer. These fluctuations are strictly nonpropagating and their self-interactions are independent of $\boldsymbol{B}_0$ and its associated propagation effects. Two-dimensional fluctuations typify the strongly interacting modes to which the driven wave is coupled.

In *un*forced RMHD, the reduced and two-dimensional spectra are expected to be very similar (after normalizing appropriately) since RMHD modes are, by definition, those for which Alfvén wave effects are not dominant. Consequently, as τ_A depends on k_z, the perpendicular spectra at

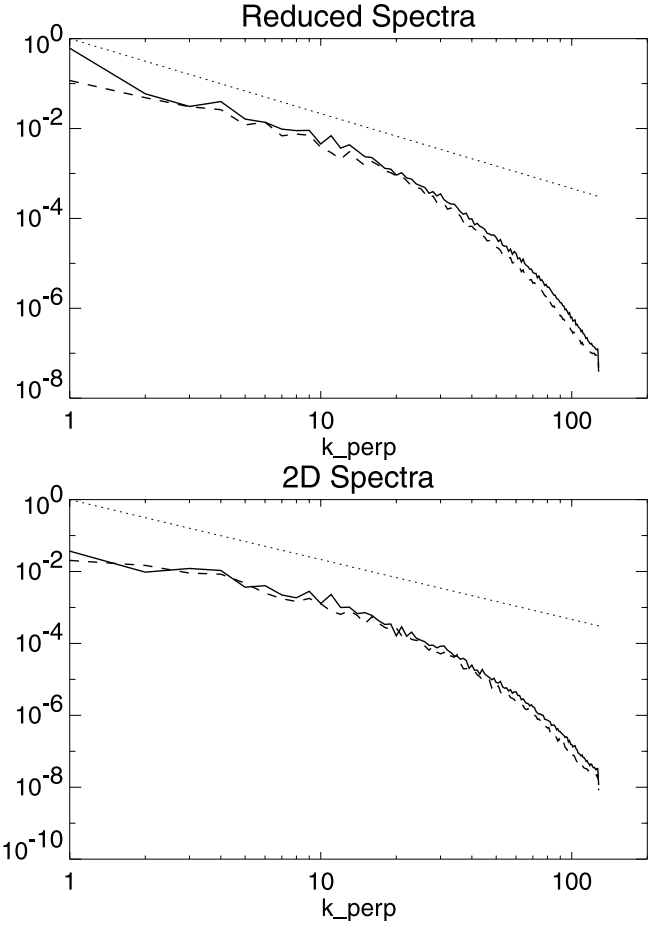

FIG. 3.—Perpendicular spectra of the fluctuation energy from the primary run at $t = 100$. Top panel is the reduced (summed over k_z) spectrum of the fluctuation energy. Kinetic (*dashed line*) and magnetic (*solid line*) energy spectra are shown separately. A $k^{-5/3}$ reference line (*dotted line*) is also shown. Lower panel shows perpendicular spectra for the two-dimensional ($k_z = 0$) components of the magnetic (*solid line*) and kinetic (*dashed line*) energy. Note that magnetic energy exceeds kinetic energy at almost every scale.

each k_z should be similar. This is seen to be the case in free-decay runs. Our driven situation differs from this since the driven mode involves a particular k_z ($=1$). The associated $E(k_\perp, k_z)$ thus contains significantly more energy than the spectra at other k_z.

The fluctuations are broadly distributed in (x-space) values as well as in wavenumber, as is typical in fully developed turbulence. In Figure 4, we show the observed distributions (probability distribution functions, or PDFs) of the electric current density, vorticity, and the x-components of the magnetic and velocity fields, b_x, v_x, for the same run as above. Clearly, the PDFs for b_x and v_x are very similar and close to Gaussian. Indeed, the kurtosis of b_x is $\kappa_{bx} = \langle b_x^4 \rangle / \langle b_x^2 \rangle^2 \doteq 3.1$, to be compared with the Gaussian value of 3. The kurtosis of v_x is also 3.1. On the other hand, the PDFs for the vorticity and the current density have highly non-Gaussian tails, suggesting that they are strongly intermittent quantities ($\kappa_\omega \doteq 5.9$, $\kappa_j \doteq 10.1$). Moreover, as the PDF for j is significantly less Gaussian than that for ω, this implies a more intermittent or bursty behavior for the current density, perhaps a consequence of the dynamics of the MHD dissipative structures. Temporal plots of total viscous and resistive dissipation show analogous results. However, the extent to which this result is general, or an artifact of the moderately high Reynolds numbers allowed by the resolution of our simulations, remains to be established.

The disparity between degrees of intermittency at large and small scales (i.e., $\boldsymbol{v}$, $\boldsymbol{b}$ vs. ω, j) is entirely expected on the basis of both hydrodynamic and MHD treatments (Nelkin 1994; Frisch 1995; Muller & Biskamp 2000). Specifically, small-scale intermittent behavior is associated with formation of characteristic small-scale coherent structures in MHD. For the two-dimensional case, these are small-scale sheets and/or filaments of electric current density along with fine-scale quadrupolar distributions of vorticity (Frisch et al. 1983; Matthaeus & Lamkin 1986; Biskamp & Welter 1989; Hendrix & van Hoven 1996; Muller & Biskamp 2000) and are associated with the formation and dynamics of small-scale reconnection regions. These are essential features of the dissipative process in two-dimensional MHD.

We illustrate the spatial structure of the fluctuations using plots of the velocity and magnetic field vectors overlaid on intensity diagrams for the vorticity and electric current density (Fig. 5). It is evident that the magnetic field and velocity structures are dominated by large-scale features that approach the box dimension in size, although there is a clear distribution across scales, consistent with Figure 3. On the other hand, the electric current and vorticity take on large values only in very small regions of space. Figure 5 shows that these small regions are of the type connected with magnetic reconnection between adjacent magnetic islands. This confirms that the characteristic small-scale features in driven RMHD are essentially the same as in two-dimensional MHD (e.g., Milano et al. 1999). Small-scale reconnection-related electric current channels and vorticity structures are responsible for intermittency and most of the dissipation in the RMHD scenario. To the extent that this picture is viable for coronal heating, these small-scale characteristic features should be relevant in that context as well. Similar conclusions have been drawn for closed field-line regions driven quasi-statically by photospheric footpoint motions (Hendrix & van Hoven 1996; Dmitruk et al. 1998).

Another contrast between the small- and large-scale features of the turbulence can be seen in correlations that are revealed by scatter plots. In Figure 6 we show two such scatter plots, obtained from the sampled time series of global quantities computed from our main driven run. The upper panel plots (global) kinetic energy $E^v(t)$ at time t versus the magnetic energy $E^b(t)$ at the same time. The lower panel plots global mean-square vorticity $\langle \omega^2 \rangle$ versus mean-square current $\langle j^2 \rangle$. Evidently there is a strong anticorrelation between kinetic and magnetic energies. This is consistent with interference between counterpropagating wave packets at low wavenumber. The slope of this anticorrelation is quite accurately -1, as demonstrated in the figure. A similar effect has been discussed by Pouquet, Frisch, & Meneguzzi (1986) for full three-dimensional MHD. On the other hand, the positive correlation between $\langle j^2 \rangle$ and $\langle \omega^2 \rangle$ clearly cannot be associated with wave propagation. However, it is well known (Matthaeus & Lamkin 1986) that small-scale reconnection involves localized production of both mean-square current and vorticity in connection with intense periods of small-scale activity near

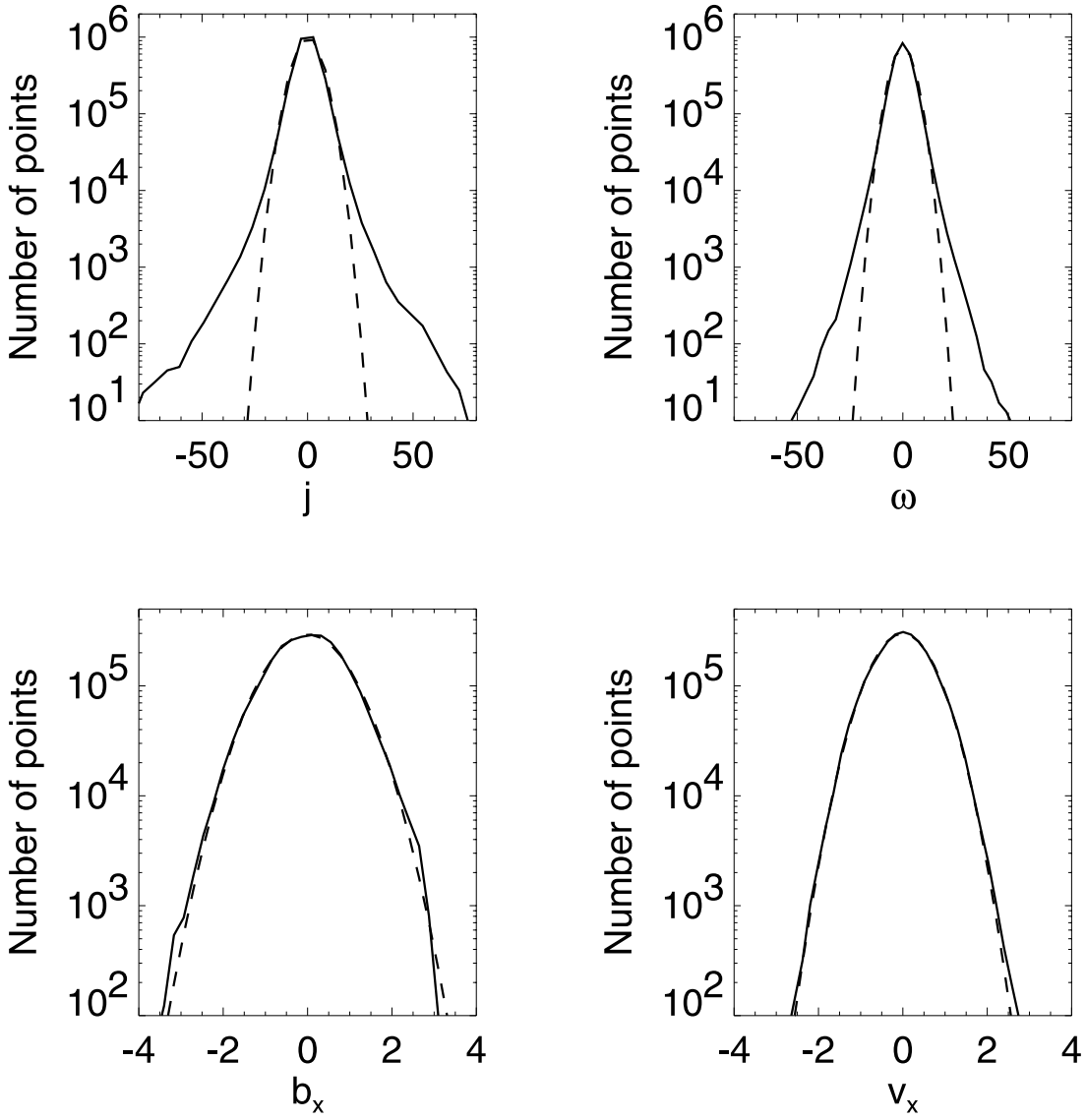

FIG. 4.—Histograms of the distribution of electric current density, vorticity, and x-components of the magnetic and velocity fields using data accumulated from snapshots at $t = 50, 100, 150, \ldots, 500$ in the primary run. Dashed curves are Gaussian best fits.

reconnection sites. We interpret the positive correlation in the bottom panel of Figure 6 as indicative of this. Thus, the strongly nonlinear dynamical features that were discussed in connection with Figures 4 and 5 provide a consistent explanation for the phenomenon seen in Figure 6.

4.3. *Cross Helicity and Reflection*

Driving occurs in our model by adding energy to a negative cross helicity Fourier mode. In the absence of reflection or nonlinearity, this would correspond to driving a large-amplitude, upward-propagating Alfvén wave. However, because seed-level turbulence and reflection are both present, the driven fluctuations experience strong nonlinear couplings. These require that both positive and negative cross helicity excitations participate—otherwise nonlinearity vanishes for RMHD. If a steady level of turbulent cascade is achieved, and we have seen that this is usually the case, there must be a steady admixture of both negative cross helicity (outward-type) and positive cross helicity (inward-type) fluctuations. It is useful to document how this mixture of cross helicities varies with reflection rate R. This is examined by computing the steady normalized cross helicity, $\sigma_c = (E^+ - E^-)/(E^+ + E^-)$, averaged over all $t \geq 50$, for fixed run parameters other than the reflection rate R.

Figure 7 shows these averages for a range of R and for a collection of two series of runs having either a $256^2 \times 4$ resolution with Reynolds numbers of 800, or a $64^2 \times 4$ resolution with Reynolds numbers of 200. Recall also that $T = 1$, so that the physically important ratio $R/T \equiv R$. One can see that for rather weak reflection the steady cross helicity is a rapidly increasing function of R. This sensitivity persists up to $R \sim 1$, at which point $\sigma_c \sim 0$, implying that inward and outward energy densities are comparable: $E^+ \approx E^-$. In fact, for reflection strengths as small as $R \sim 0.1$, the inward energy E^+ is about 25% of the total fluctuation energy. Evidently it is a feature of the present model that substantial turbulent heating usually corresponds to a substantial steady state flux of inward-type fluctuations. The counterpropagating fluctuations are strongly interacting, as is evidenced by the substantial heating rates observed (see § 4.4).

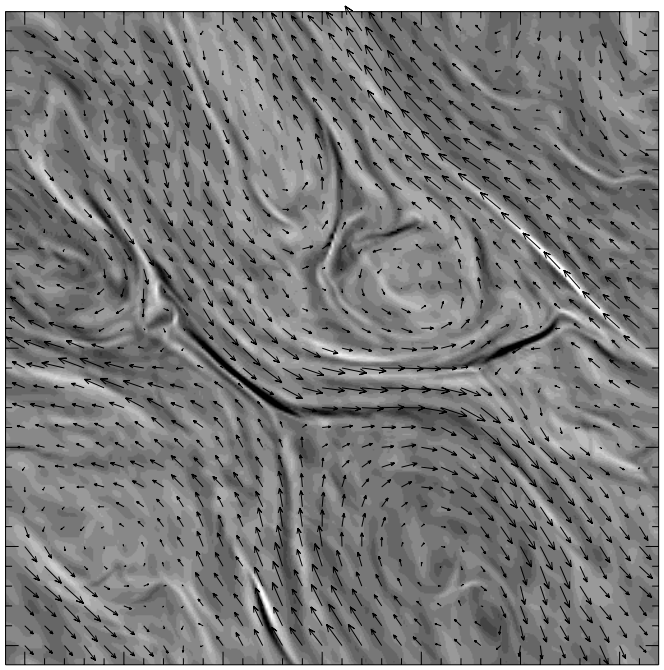

FIG. 5*a*

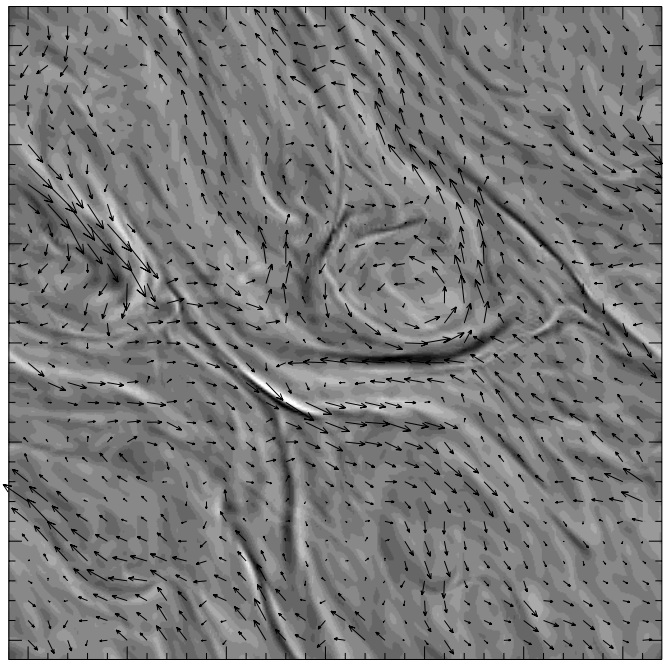

FIG. 5*b*

FIG. 5.—Some fields from a perpendicular cross section of the primary run at $t = 100$. (*a*) Intensity plot of electric current density. Overlaid arrows are the transverse magnetic field fluctuations. (*b*) Intensity plot of vorticity ω. Overlaid arrows are the velocity field fluctuations in the transverse plane.

Also shown on the figure is the situation when $R = 0$. In this case, the asymptotic steady σ_c is -1, corresponding to pure outward propagation and no turbulence. This special case is discussed further below.

4.4. *Heating and Reflection*

It is also of interest to investigate the variation of the steady state heating rate with reflection strength. We use the same set of runs represented by the data in Figure 7—recalling that the runs have Reynolds numbers of either 200 or 800. Figure 8 displays the time-averaged energy loss rates associated with transmission of energy out of the domain (TE^-) and with turbulent dissipation ($\epsilon_{\rm turb}$) as a function of reflection rate. Steady dissipation rates exceeding 0.2 are attained for all reflection rates higher than about $R = 0.1$. The sum of the transmitted energy loss rate and the dissipation rate is approximately unity, a consequence of setting the energy supply rate $F = 1$ for all the driven runs. Thus the "efficiency," defined as $\epsilon_{\rm turb}/F$, which is the fraction of energy channeled through turbulent heating, is also observed to be 20% or more whenever $R > 0.1$. The point $R = 0$ is singular, and the efficiency is a steep function of R as $R \to 0$, consistent with the discussions presented in connection with Figures 7 and 9. One should also note that Figure 8 is qualitatively completely consistent with the heating rates and efficiencies found by Matthaeus et al. (1999), wherein heating rates were based on a phenomenological turbulence model rather than the explicit treatment employed here (the quantitative agreement is also rather good).

4.5. *Initial Turbulence Level*

As already noted, when $R = 0$ the turbulent dissipation and heating tend to zero. The approach to this final state is illustrated in Figure 9, which shows the time history of the dissipation experienced by all modes other than the driven mode (curve labeled $R = 0$), that is, the total dissipation through both magnetic and kinetic channels, corrected by subtracting the dissipation experienced by the single forced Fourier mode (the *direct* dissipation of the forced mode's energy is clearly distinct from the dissipation associated with a turbulent cascade). This is a $64^2 \times 4$ simulation with an initial seed turbulence energy level of $E = 1$. There is a burst of turbulent dissipation very early on, followed by an approximately power-law decay that persists until $t \approx 40$. After that, the turbulent dissipation decays exponentially. Thus we conclude that when $R = 0$, the time-asymptotic turbulent dissipation rate is also zero.

All runs discussed so far have had unit fluctuation energy, $E = 1$, and zero cross helicity, $E^+ = E^- = \frac{1}{2}$, at $t = 0$. This more or less arbitrary level of initial turbulence has been used to trigger subsequent nonlinear activity driven by the (externally supplied) wave energy. A natural question to investigate at this point is whether the level of turbulent dissipation attained in the final steady state is sensitive to the initial turbulence level. To examine this, we carried out a set of $64^2 \times 4$ simulations with varying initial energy levels. The energy is distributed across the same (broadband) set of wavevectors in each case with the cross helicity near zero. Other parameters, including the reflection rate $R = \frac{1}{2}$ and the Reynolds numbers $\mathrm{Re} = R_m = 200$, were identical from run to run. Figure 9 illustrates the results of three runs from this series. Shown are the turbulent dissipation rates (total dissipation minus dissipation in the forced mode) versus time for runs with initial turbulence levels of $E_0 = 1$, $\frac{1}{10}$, and 10^{-5}. One can see that for the lower values of E_0, the dissipation rate increases over a timescale of $\approx 20\tau_{\rm nl}$ and subsequently attains essentially the same rate of dissipation in each case.

Evidently the steady state level of turbulent dissipation is robust and not sensitive to the initial (seed) turbulence level. As mentioned earlier, a zero level of initial turbulence leads

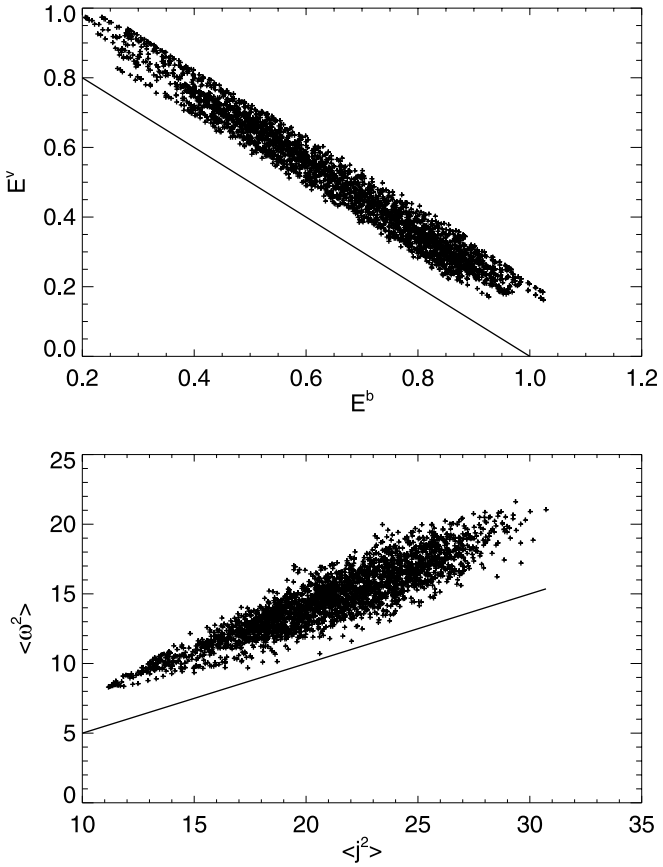

FIG. 6.—Scatter plots of (*top*) kinetic energy vs. magnetic energy, and (*bottom*) mean-square vorticity vs. mean-square current density. Data points are from the primary run with $10 \leq t \leq 250$. The latter shows a strong correlation at all but the lowest values, indicative of small-scale *non*wavelike activity that we attribute to small-scale current and vorticity structures associated with magnetic reconnection. The former portrays a strong anticorrelation throughout, consistent with the presence of (counterpropagating) waves at low wavenumber. Lines with slope -1 (*top*) and $+1/2$ (*bottom*) are shown for reference.

to a simple propagating wave solution even when reflection is present. In that case, there is no spectral transfer, no cascade, and no turbulent dissipation. However, even an extremely small amount of initial turbulence is sufficient to

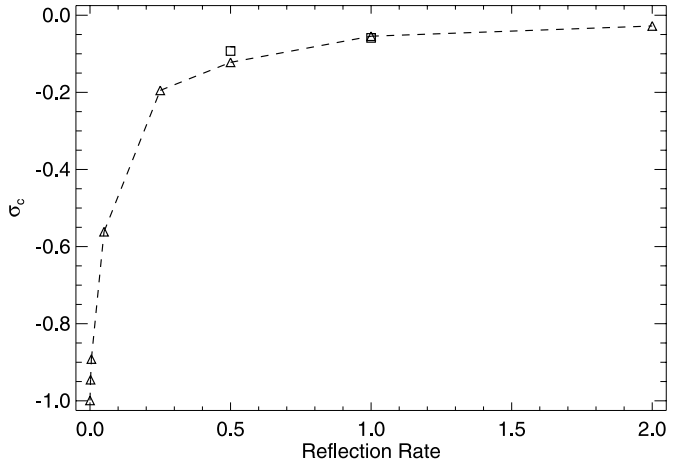

FIG. 7.—Steady values of σ_c, the normalized cross helicity, for a series of $64^2 \times 4$ (*triangles*) and $256^2 \times 4$ (*squares*) runs plotted vs. the reflection rate R.

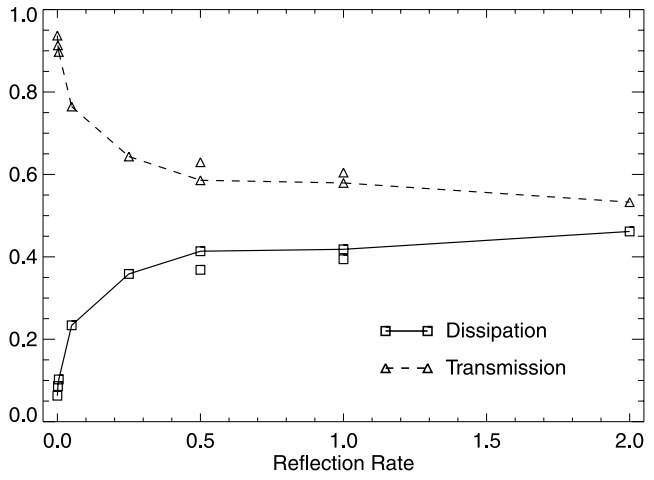

FIG. 8.—Steady energy loss rates caused by dissipation and transmission averaged over all $t \geq 50$ as a function of R. Results from a family of runs at resolution $64^2 \times 4$ with large-scale Reynolds number of $\mathrm{Re} = 200$ are shown connected by lines. Results from the two $256^2 \times 4$ runs ($\mathrm{Re} = 800$) are shown as unconnected squares and triangles.

trigger nonlinear couplings that regenerate the turbulence to a robustly recurring level. This property, which suggests that the $E(t = 0) \rightarrow 0$ case is a singular limit, indicates that the highly turbulent state is strongly favored in the present model.

5. DISCUSSION

There are at least four important characteristics of the heating mechanism presented here that heating models based on direct wave damping can lack. First, since the heating occurs via *indirect* damping of the driving Alfvén waves (which propagate either upward or downward), the restrictive constraints associated with "box-crossing" timescales play no important role. All that is required is that

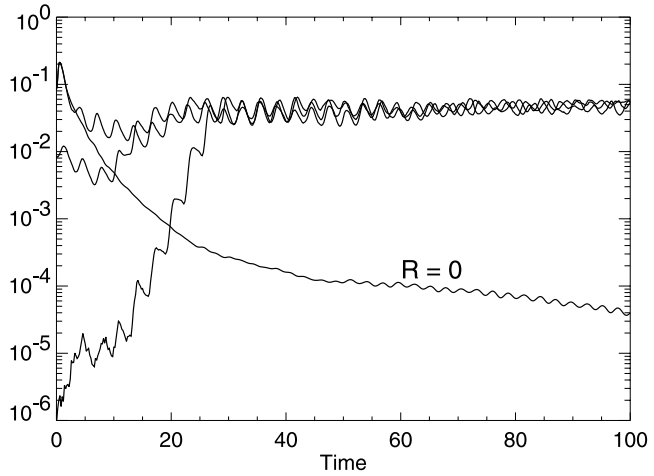

FIG. 9.—Time history of total dissipation (Ohmic plus viscous) for several $64^2 \times 4$ runs. Contribution of the self-dissipation of the driven mode is subtracted out in each case. The trace labeled $R = 0$ is for a run with initial energy $E_0 = 1$ and *no* reflection. The energy decays smoothly and no steady turbulent dissipation is attained. The top curve is for an identical run, aside from the value of the reflection parameter, $R = \frac{1}{2}$. Dissipation reaches a steady state after about $t = 20$ nonlinear times. The two other curves are for $R = \frac{1}{2}$ and identical other initial parameters except the initial turbulence level, which is set to either $E_0 = \frac{1}{10}$ or $E_0 = 10^{-5}$. For fixed R, essentially the *same* steady state dissipative level is attained independent of E_0.

enough energy be bled out of the propagating wave population to sustain the quasi–two-dimensional turbulence. As waves are constantly being generated—at the coronal base and by reflection—the reservoir of energy driving the turbulence is maintained.

In this context, recall that the dissipation rate associated with a (statistically steady) turbulent cascade of energy is set by the energy injection rate (a fixed constant in our simulations). The energy cascade acts as a "pipeline" between the large energy-injection scales and the small dissipative scales. For roughly steady driving of the turbulence, the timescale for transit of the pipeline is the large-scale eddy-turnover time $\tau_{\rm nl} = \lambda_\perp/\sqrt{E}$, where E is the energy in the turbulence and $\lambda_\perp$ is a characteristic length scale for, in this case, the quasi–two-dimensional turbulence. This result is independent of the Reynolds numbers (e.g., Lesieur 1990; Frisch 1995) and also of the periods of the driving waves, except insofar as the nonlinear interaction time for the counterpropagating waves is period dependent.

Another characteristic of a reflection-driven model is that the plasma heating occurs essentially "in place," that is, at much the same height at which the wave energy is injected into the quasi–two-dimensional component. Two factors contribute here: (1) the speed of the nascent solar wind is inferred to be low in the region where the heating process is most relevant (Grall et al. 1996; Guhathakurta et al. 1999; Sittler & Guhathakurta 1999), ensuring that advection does not move the energy very far outward spatially as it undergoes spectral transfer to small perpendicular scales; and (2) although the quasi–two-dimensional fluctuations have long parallel ($\approx$ vertical) length scales, the energy transfer to them is initiated at the heights where the upward and downward modes spatially overlap. While this region is relatively extended, given that factor (1) holds, the cascade and heating will still take place in approximately the same height range.

A third important feature is that the dynamics of quasi–two-dimensional turbulence is essentially insensitive to the mean field strength, B_0 (e.g., Oughton et al. 1994; Hossain et al. 1995; Matthaeus et al. 1996; Kinney & McWilliams 1998; Matthaeus et al. 1998; Oughton et al. 1998). In particular, the associated nonlinear timescale is approximately independent of B_0, provided that $E/B_0^2 \lesssim 1$. This condition is expected to hold in the corona. Thus, once the energy has been injected into the turbulence, the heating process depends only weakly on B_0. The injection process itself—which involves competition between reflection, transmission, and nonlinear interactions—clearly depends on gradients of $\boldsymbol{B}_0$ but may not depend strongly on the field strength. We note that various observed quantities also show (approximate) solar cycle independence, e.g., coronal (hole) temperature, solar-wind mass flux, and maximum fast solar wind speed.

Finally, because the non-WKB reflection is more effective for lower frequency waves (Moore et al. 1991; Musielak, Fontenia, & Moore 1992; Velli 1993), the present model is most efficient when driven by such modes. Observations and informed estimates indicate that there is adequate energy available to heat the corona in this portion of the power spectrum; the problem has been finding mechanisms that can successfully extract it. On the other hand, evidence for sufficient power at higher frequencies is currently scant (McKenzie et al. 1995; Axford & McKenzie 1997; Tu & Marsch 1997; Spangler & Mancuso 2000).

Although the spectrum of coronal fluctuations is unknown, there is growing evidence that their energy content is substantial. Chae, Schühle, & Lemaire (1998) have offered evidence for turbulent fluctuations with amplitudes ~ 30 km s^{-1} in the lower corona. There has also been the suggestion (Hassler et al. 1990) that the observed increase with altitude of the associated nonthermal line broadening, and subsequent saturation at about 1.1 to 1.2 $R_\odot$, may signify reflection and/or damping of the turbulent fluctuations. Observations at somewhat higher altitudes (~ 1.5–$3\ R_\odot$) from both *SPARTAN* (Kohl et al. 1995) and the Ultraviolet Coronagraph and Spectrometer on the *Solar and Heliospheric Observatory* (Kohl et al. 1997) support the interpretation that protons are heated to several million degrees K. This would appear to be consistent with a turbulent heating mechanism that commences at slightly lower altitudes. However, there is also an inherent ambiguity in some of these observations since contributions to line broadening from fluctuations and from thermal motions are difficult to disentangle (Cranmer, Field, & Kohl 1999), even in the case of inferred anisotropy (Kohl et al. 1998).

The distinction between propagating fluctuations and turbulence has also gained some attention in recent observations. Upward wave fluxes are detected in the chromosphere (Ulrich 1996) while detection of wave fluxes in the transition region (Doyle et al. 1998) is less definitive at present. As for the corona, Chae et al. (1998) argue that upward waves are *not* present, and they prefer to interpret their results in terms of small-scale MHD turbulence. It is not clear to us if these observations are conclusive or if they might be consistent with a mixture of positive and negative cross helicity fluctuations that are strongly coupled, such as those we have described in our simulation model. A random mixture of upward- and downward-moving fluctuations could, presumably, cause some phase correlation tests to produce a result that could be interpreted as nonpropagation. In the context of our model, this would be consistent with the presence of strong turbulence, but from our perspective, we would not rule out the presence of low-frequency propagating waves that may drive the system. However, in steady state, our model would suggest that substantial reflection results in near equal admixtures of inward- and outward-type signals. Indeed, this characteristic would appear to be one that distinguishes the high-frequency wave-driven models (Axford & McKenzie 1997) from the present low-frequency model. The former have no mechanism or requirement involving an inward propagating component. On the other hand, our model appears to require a steady inward admixture of fluctuations, thus providing an observational basis for distinguishing the models.

It is interesting to note that the heating mechanism discussed herein may also be relevant in magnetically closed regions such as coronal loops. The essential elements of the mechanism are the presence of both (low-frequency) counterpropagating Alfvén waves and (seed-level) turbulence in the planes perpendicular to the large-scale magnetic field. Many closed field-line heating models also rely on the interaction of countertraveling disturbances (generated, for example, by photospheric footpoint motions at each end of a coronal loop). As in the present model, these waves could then couple to quasi-perpendicular fluctuations with a subsequent cascade of the energy to small scales and eventual conversion into heat (e.g., Gómez & Ferro-Fontán 1992;

Heyvaerts & Priest 1992; Velli 1996; Hendrix & van Hoven 1996; Einaudi et al. 1996; Dmitruk et al. 1998; Priest et al. 1998). There is then the suggestion that the same heating mechanism is active in both types of field-line regions, with the major difference being the way in which the counter-propagating Alfvénic fluctuations are generated, i.e., reflection versus boundary motions.

In conclusion, the present results, based on direct numerical simulation, support our earlier suggestion that turbulence driven by low-frequency waves and reflection may provide a viable heating mechanism for the open field-line corona. In addition to further examination of observational constraints, we plan to develop this model further by incorporating more realistic models of the coronal field, self-consistent reflection, and more realistic open boundary conditions.

This work is supported by NASA grants NAG 5-7164, NAG 5-8134 (SEC Theory Program), and NSF grant ATM 97-13595 to the Bartol Research Institute, and PPARC grant PPA/G/S/1999/00059.

REFERENCES

Axford, W. I., & McKenzie, J. F. 1997, in Cosmic Winds and the Heliosphere, ed. J. R. Jokipii, C. P. Sonett, & M. S. Giampapa (Tucson: Univ. Arizona Press), 31
Berger, T. E., & Title, A. M. 1996, ApJ, 463, 365
Bhattacharjee, A., Ng, C. S., & Spangler S. R. 1998, ApJ, 494, 409
Biskamp, D., & Welter H. 1989, Phys. Fluids B, 1, 1964
Carbone, V., & Veltri, P. 1990, Geophys. Astrophys. Fluid Dyn., 52, 153
Chae, J., Schühle, U., & Lemaire, P. 1998, ApJ, 505, 957
Cranmer, S. R., Field, G. B., & Kohl, J. L. 1999, ApJ, 518, 937
Davila, J. M. 1987, ApJ, 317, 514
Dmitruk, P., & Gómez, D. O. 1999, ApJ, 527, L63
Dmitruk, P., Gómez, D. O., & DeLuca, E. E. 1998, ApJ, 505, 974
Doyle, J. G., den Oord, G. H. J. V., O'Shea, E., & Banerjee, D. 1998, Sol. Phys., 181, 51
Doyle, J. G., O'Shea, E., Erdelyi, R., Dere, K. P., Socker, D. G., & Keenan, F. P. 1997, Sol. Phys., 173, 243
Einaudi, G., Velli, M., Politano, H., & Pouquet, A. 1996, ApJ, 457, L113
Frisch, U. 1995, Turbulence (Cambridge: Cambridge Univ. Press)
Frisch, U., Pouquet, A., Sulem, P.-L., & Meneguzzi, M. 1983, J. de Mécanique Théorique et Appliquée, 216, 191
Gazol, A., Passot, T., & Sulem, P. L. 1999, Phys. Plasmas, 6, 3114
Ghosh, S., Matthaeus, W. H., Roberts, D. A., & Goldstein M. L. 1998a, J. Geophys. Res., 103, 691
———. 1998b, J. Geophys. Res., 103, 705
Gómez, D. O., & Ferro-Fontán, C. 1992, ApJ, 394, 662
Grall, R. R., Coles W. A., Klinglesmith, M. T., Breen, A. R., Williams, P. J. S., Markkanen, J., & Esser, R. 1996, Nature, 379, 429
Guhathakurta, M., Sittler, E. C., Fisher, R., McComas, D., & Thompson, B. 1999, Geophys. Res. Lett., 26, 2901
Hassler, D. M., Rottman, G. J., Shoub, E. C., & Holzer, T. E. 1990, ApJ, 348, L77
Hendrix, D., & van Hoven, G. 1996, ApJ, 467, 887
Heyvaerts, J., & Priest, E. R. 1983, A&A, 117, 220
———. 1992, ApJ, 390, 297
Hollweg, J. V. 1981, Sol. Phys., 70, 25
———. 1984, ApJ, 277, 392
———. 1996, in Solar Wind Eight, ed. D. Winterhalter, J. T. Gosling, S. R. Habbal, W. S. Kurth, & M. Neugebauer (New York: AIP), 327
———. 1997, ApJ, 488, 895
Hossain, M., Gray, P. C., Pontius, D. H., Jr., Matthaeus, W. H., & Oughton, S. 1995, Phys. Fluids, 7, 2886
Hossain, M., Vahala, G., & Montgomery, D. 1985, Phys. Fluids, 28, 3074
Hu, Y. Q., Esser, R., & Habbal, S. R. 1997, J. Geophys. Res., 102, 14661
Khabibrakhmanov, I., & Mullan, D. 1997, ApJ, 488, 898
———. 1994, ApJ, 430, 814
Kinney, R., & McWilliams, J. C. 1998, Phys. Rev. E, 57, 7111
Kohl, J. L., et al. 1995, Space Sci. Rev., 72, 29
———. 1997, Sol. Phys., 175, 613
———. 1998, ApJ, 501, L127
Leamon, R. L., Matthaeus, W. H., Smith, C. W., Zank, G. P., Mullan, D. J., & Oughton, S. 2000, ApJ, 537, 1054
Lesieur, M. 1990, Turbulence in Fluids (Dordrecht: Nijhoff)
Longcope, D. W., & Sudan, R. N. 1994, ApJ, 437, 491
Matthaeus, W. H., Ghosh, S., Oughton, S., & Roberts, D. A. 1996, J. Geophys. Res., 101, 7619
Matthaeus, W. H., & Lamkin, S. L. 1986, Phys. Fluids, 29, 2513
Matthaeus, W. H., Oughton, S., Ghosh, S., & Hossain, M. 1998, Phys. Rev. Lett., 81, 2056
Matthaeus, W. H., Zank, G. P., Oughton, S., & Mullan, D. J. 1999, ApJ, 523, L93
McKenzie, J., Banaszkiewicz, M., & Axford, W. I. 1995, A&A, 303, L45
Mikić, Z., Schnack, D. D., & Van Hoven, G. 1989, ApJ, 338, 1148
Milano, L. J., Dmitruk, P., Mandrini, C. H., & Gómez, D. O. 1999, ApJ, 521, 889
Montgomery, D. C. 1982, Phys. Scr., 2, 83
Montgomery, D. C., & Turner, L. 1981, Phys. Fluids, 24, 825
Moore, R. L., Musielak, Z. E., Suess, S. T., & An C.-H. 1991, ApJ, 378, 347
Muller, W.-C., & Biskamp, D. 2000, Phys. Rev. Lett., 84, 475
Musielak, Z. E., Fontenia, J. M., & Moore, R. L. 1992, Phys. Fluids B, 4, 13
Nelkin, M. 1994, Adv. Phys., 43, 143
Ofman, L., Davila, J. M., & Steinolfson, R. S. 1994, ApJ, 421, 360
Ofman, L., & DeForest, C. E. 2000, Adv. Space Res., 25, 1909
Ofman, L., Nakariakov, V. M., & Sehgal, N. 2000, ApJ, 533, 1071
Oughton, S., Ghosh, S., & Matthaeus, W. H. 1998, Phys. Plasmas, 5, 4235
Oughton, S., Matthaeus, W. H., Zank, G. P., & Mullan, D. J. 1999, in Plasma Dynamics and Diagnostics in the Solar Transition Region and Corona, ed. J.-C. Vial & B. Kaldeich-Schürmann (ESA SP-446), 525
Oughton, S., Priest, E. R., & Matthaeus, W. H. 1994, J. Fluid Mech., 280, 95
Parker, E. N. 1991, ApJ, 372, 719
Pouquet, A., Frisch, U., & Meneguzzi, M. 1986, Phys. Rev. A, 33, 4266
Priest, E. R., Foley, C. R., Heyvaerts, J., Arber, T. D., Culhane, J. L., & Acton, L. W. 1998, Nature, 393, 545
Shebalin, J. V., Matthaeus, W. H., & Montgomery, D. 1983, J. Plasma Phys., 29, 525
Sittler, E. C., & Guhathakurta, M. 1999, ApJ, 523, 812
Spangler, S. R., & Mancuso, S. 2000, ApJ, 530, 491
Strauss, H. R. 1976, Phys. Fluids, 19, 134
Tu, C.-Y., & Marsch, E. 1997, Sol. Phys., 171, 363
Ulrich, R. K. 1996, ApJ, 465, 436
Velli, M. 1993, A&A, 270, 304
———. 1996, in Solar Wind Eight, ed. D. Winterhalter, J. T. Gosling, S. R. Habbal, W. S. Kurth, & M. Neugebauer (New York: AIP), 28
Warren, H. P., Mariska, J. T., Wilhelm, K., & Lemaire, P. 1997, ApJ, 484, L91
Zank, G. P., & Matthaeus, W. H. 1992, J. Plasma Phys., 48, 85
Zhou, Y., & Matthaeus, W. H. 1990a, J. Geophys. Res., 95, 291
———. 1990b, J. Geophys. Res., 95, 863